Catalysis Letters (2018) 148:1472–1477
https://doi.org/10.1007/s10562-018-2325-4

Mono and Bimetallic Pt–(M)/Al_2O_3 Catalysts for Dehydrogenation of Perhydro-*N*-ethylcarbazole as the Second Stage of Hydrogen Storage

Andrey L. Tarasov[1,2] · Olga P. Tkachenko[1] · Leonid M. Kustov[1,2,3]

Received: 4 April 2016 / Accepted: 5 February 2018 / Published online: 7 March 2018

Abstract
The comparative study of the activity of mono- and bimetallic Pt–(M)/Al_2O_3 catalysts in perhydro-*N*-ethylcarbazole dehydrogenation as the second stage of hydrogen storage (hydrogen release) has been performed. It has been found that the activity of a Pt/Al_2O_3 catalyst can be enhanced via the second metal (Cr, Pd) introduction. This fact gives the possibility to use Pt–(M)/Al_2O_3 catalysts for the hydrogen storage process based on reversible cycles of hydrogenation–dehydrogenation of aromatic substrates. X-ray absorption spectroscopy (XANES and EXAFS) revealed that Cr introduction impacts the electronic state and local environment of Pt. The average size of platinum metal nanoparticles is about two times smaller in Pt–Cr/Al_2O_3 compared to Pt/Al_2O_3.

✉ Leonid M. Kustov
lmk@ioc.ac.ru

[1] N.D. Zelinsky Institute of Organic Chemistry, Russian Academy of Sciences, 47 Leninsky prospect, 119991 Moscow, Russia

[2] National University of Science and Technology MISiS, Leninsky prosp. 4, Moscow, Russia

[3] Chemistry Department, Moscow State University, Leninskie Gory 1, bldg. 3, 119992 Moscow, Russia

Graphical Abstract

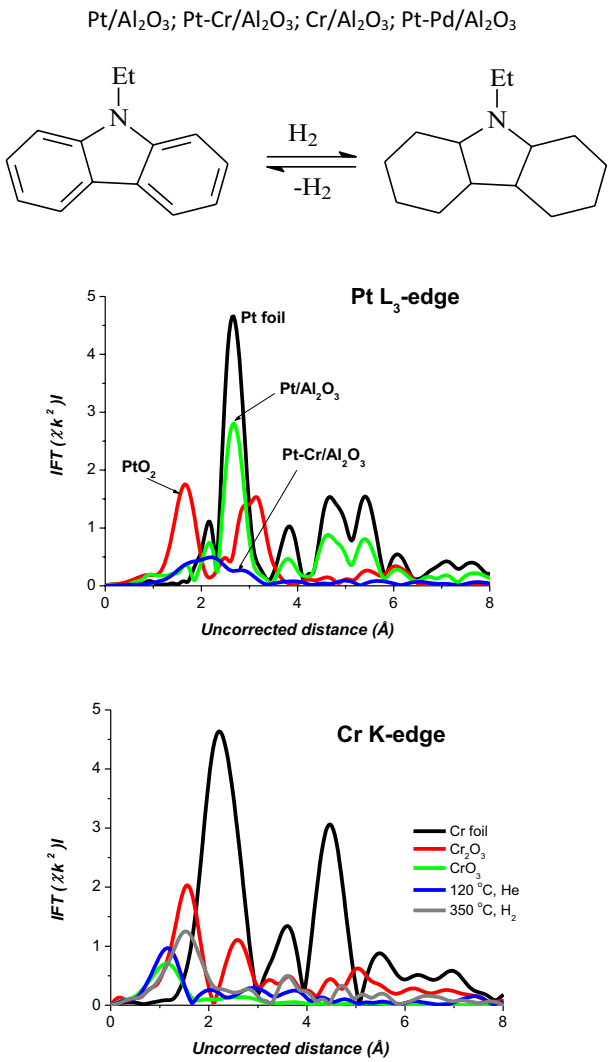

Keywords Dehydrogenation · Perhydro-*N*-ethylcarbazole · Pt-containing catalysts · X-ray absorption spectroscopy · Hydrogen storage

1 Introduction

Presently hydrogen is regarded as one of the main energy sources for environment friendly transport. Herewith the solution of the problem of efficient H_2 storage would result in a real alternative to liquid fuels (gasoline and diesel). A very effective approach to the hydrogen storage problem is based on the reversibility of hydrogenation–dehydrogenation reactions of aromatics and heterocycles. Condensed polycyclic aromatic hydrocarbons or heteroaromatic moieties containing nitrogen, oxygen or other heteroatoms are considered as substrates fort his method of hydrogen storage. The conjugated substrates can be pyrenes, coronenes, indenes, carbazole derivatives etc [1]. The pair of *N*-ethylcarbazole and perhydro-*N*-ethylcarbazole is one of the promising systems, because as much as 5.8 wt% of hydrogen can be taken up and released in the consecutive hydrogenation and dehydrogenation reactions [2]. Moreover, it was found [3] that the perhydro-*N*-ethylcarbazole dehydrogenation heat is about 50 kJ/mol H_2, that allows to carryout the dehydrogenation reaction at temperatures lower than 200 °C. Pd-containing catalysts supported on activated carbon, SiO_2, and TiO_2 were studied using this substrate pair [4–6]. The objective of this study is the study of the effect of modification of Pt/Al_2O_3

catalysts by some non-noble (Cr) and noble (Pd) second components on the activity of the perhydro-*N*-ethylcarbazole dehydrogenation reaction. The choice of the second metal is based on the ability to catalyze dehydrogenation reactions. Since chromium is much less active compared to palladium, the concentration of Cr in the catalyst was much higher (0.5 wt%) compared to that of Pd (0.1 wt%), but still lower than that of the main metal—Pt (1 wt%).

2 Experimental

2.1 Materials

A Pt/Al_2O_3 catalyst was prepared by incipient wetness impregnation of γ-Al_2O_3 (A-64 trademark, Ryazan Refinery, 0.1–0.2 mm fraction) using an H_2PtCl_6 aqueous solution followed by drying in air at 90 °C. Bimetallic Pt–Cr/Al_2O_3 and Pt–Pd/Al_2O_3 catalysts were prepared by incipient wetness impregnation of Pt/Al_2O_3 using $(NH_4)_2Cr_2O_7$ and $[Pd(NH_3)_4]Cl_2$ aqueous solutions, correspondingly. After drying in air at 90 °C, the catalysts were calcined in air at 500 °C and reduced in an H_2 flow at 350 °C for 2 h. Then the catalysts were placed under Ar into a static reactor and perhydro-*N*-ethylcarbazole (H_{12}–NEC) was added.

2.2 Dehydrogenation of perhydro-*N*-ethylcarbazole (H_{12}–NEC)

The scheme of hydrogenation–dehydrogenation reactions of perhydro-*N*-ethylcarbazole (H_{12}–NEC) is shown below:

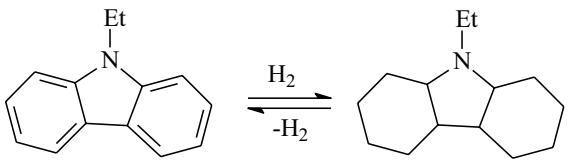

The catalyst (0.25 g) and H_{12}–NEC (1.0 g) were placed in a batch reactor (a glass vessel, 10 ml volume), the reactor was heated at ambient atmosphere up to 195 °C, and the reaction mixture was kept at this temperature with stirring at 600 rpm for 6 h.

2.3 Reaction Products Analysis

The liquid products were diluted by benzene and analyzed by means of gas chromatography (a "Crystallux" chromatograph) using a capillary column SE-30 (25 m) and a flame-ionization detector at a programmed temperature regime (70 °C isotherm for 4 min, then an increase of temperature, 8 °C/min up to 180 °C). The identification of liquid hydrocarbons was done using Thermo Focus GC (Thermo TR-5MS column) connected with Thermo DSQ II mass-spectrometer. Scanning range—35–350 amu, scan rate—5 per second. The gaseous products (generally H_2 with C_1–C_2 admixtures) were collected in a gas burette (which is measured by the total amount of released hydrogen) and analyzed by using the same chromatograph at 30 °C. The dehydrogenation degree was calculated from the amount of H_2 released by dehydrogenation divided by the amount corresponding to completed hydrogenation of 1 g of H_{12}–NEC (650 ml of hydrogen).

2.4 Characterization

X-ray absorption spectra (Pt L_3 edge at 11,564 eV and Cr *K* edge at 5989 eV) were measured in a transmission mode at the HASYLAB X1 station (DESY, Hamburg, Germany) using a Si(111) double crystal monochromator (detuned to give 50% of the maximum intensity for higher harmonics suppression). The experiments were performed with an in situ cell. In a typical experiment, a sample was heated in flowing He at 120 °C and diluted hydrogen (5% in He) to the first reduction temperature at 5 °C min^{-1} and then it was kept at this reduction temperature for 15 min (stationary reduction regime). After cooling to the liquid nitrogen temperature, the spectrum of the absorption coefficient μ was taken twice (recording simultaneously the spectrum of a Pt(Cr) foil between the second and third ionization chambers for energy calibration). Subsequently, the sample was heated to the previous reduction temperature at 10 °C min^{-1} and the next temperature was established with the rate 5 °C min^{-1}. Data treatment was carried out using the software package VIPER [7]. A Victoreen polynomial was fitted to the pre-edge region for background subtraction. The smooth atomic background μ_0 was estimated using a smoothing cubic spline. The Fourier analysis of the k^2-weighted experimental function $\chi = (\mu - \mu_0)/\mu_0$ was performed with a Kaiser window. For the determination of structural parameters, theoretical references calculated by the FEFF8.10 code [8] for Cr-foil, Cr_2O_3, CrO_3, Pt-foil, and PtO_2 were used. To minimize the number of free parameters, equal backscatters were fitted with the same E_o shift wherever possible. The fitting was done in the *k*- and *r*-spaces. The shell radius *r*, coordination number *N*, Debye–Waller factor σ^2 and the adjustable "muffin-tin zero" ΔE values were determined as fitting parameters. The errors in determining the fitting parameters were found by decomposition of the statistical χ^2 function near its minimum, taking into account the maximal pair correlations.

The formal average Pt metal particle size was calculated using formula from [9], the calculation procedure was described earlier [10].

3 Results and Discussion

3.1 Dehydrogenation Reaction

According to chromato-mass-spectrometry data, the reaction mixture contained three intermediate products: H_{10}-*N*-ethylcarbazole, H_6-*N*-ethylcarbazole, and H_2-*N*-ethylcarbazole together with totally dehydrogenated *N*-ethylcarbazole. For instance, in the case of the Pt–Pd/Al_2O_3 catalyst (195 °C, 6 h), the mixture contained H_{10}-*N*-ethylcarbazole—5.8 wt%; H_6-*N*-ethylcarbazole—1.9 wt%, and H_2-*N*-ethylcarbazole—2.6 wt%, along with the desired product *N*-ethylcarbazole—89.7 wt%. Therefore the average conversion is below 89.7% (75%). This fact shows that during the dehydrogenation reaction, sequential formation of intermediate products takes place following subsequent dehydrogenation. The performances of the catalysts are presented in Table 1.

The introduction of a second component results in an increase of the catalytic activity compared to that of Pt/Al_2O_3 (Table 1). Both Pt–Cr/Al_2O_3 and Pt–Pd/Al_2O_3 catalysts provide after a prolonged time (over 10 h) the complete dehydrogenation of H_{12}-*N*-ethylcarbazole, while the Pt/Al_2O_3 catalyst is not capable to overcome the limit of 71% under the chosen conditions (195 °C).

In addition, bimetallic catalysts show a higher selectivity toward the dehydrogenation reaction, with much lower concentrations of by-products (methane and ethane) in evolving hydrogen. This parameter was considered most important in view of the potential application of the bimetallic catalysts in cyclic hydrogen storage by consecutive hydrogenation of NEC and dehydrogenation of H-NEC, since the formation of light products as a result of cracking or hydrocracking/hydrogenolysis, like methane and ethane will reduce the potential hydrogen storage capacity of the substrates, especially if the life time of over 1000 or more cycles of hydrogenation–dehydrogenation is to be taken into account. Therefore the Pt–Cr/Al_2O_3 catalyst can be a preferred choice, even in comparison with the Pt–Pd/Al_2O_3 catalyst, because (1) it is characterized by much lower concentrations of light gases formed at the dehydrogenation stage, (2) chromium is a non-noble metal unlike Pd, (3) the overall activities of the Pt–Cr and Pt–Pd catalysts are comparable. Thus, this particular catalyst was studied in detail by XAS spectroscopy.

Table 1 Dehydrogenation of perhydro-*N*-ethylcarbazole at 195 °C catalyzed by mono- and bimetallic Pt-containing catalysts

Catalysts	Time of partial dehydrogenation required to reach the indicated conversion (min)			Content of CH_4 (ppm)	Content of C_2H_6 (ppm)
	25 (%)	50 (%)	75 (%)		
Pt/Al_2O_3	156	258	n/a[a]	220	160
Pt–Pd/Al_2O_3	125	171	346	165	70
Pt–Cr/Al_2O_3	131	193	374	120	50
Cr/Al_2O_3	n/a[a]	n/a[a]	n/a[a]	–	–

[a]Not achieved

3.2 X-ray Absorption Spectroscopy

The bimetallic Pt–Cr/Al_2O_3 and monometallic Pt/Al_2O_3 catalysts were selected for the comparative study of the effect of the second component on the electronic state and local structure of platinum by X-ray absorption spectroscopy, because the effect of Cr is more pronounced in terms of the dehydrogenation selectivity and suppression of the formation of by-products (methane and ethane). In addition, the monometallic Cr-containing catalyst does not show any activity in this reaction.

The Pt L_3 X-ray absorption near-edge spectra (Fig. 1) of the Pt/Al_2O_3 and Pt–Cr/Al_2O_3 samples reduced at 350 °C demonstrate that XANES spectra of these catalysts are similar to Pt-foil regarding the energetic position and "white" line intensity.

Fourier transformation of the oscillating part of the spectrum (EXAFS, Fig. 2) of the Pt/Al_2O_3 catalyst differs from Pt-foil only in the double peak intensity. This demonstrates that platinum in this sample is completely reduced. At the same time, the EXAFS spectrum of Pt–Cr/Al_2O_3 shows that

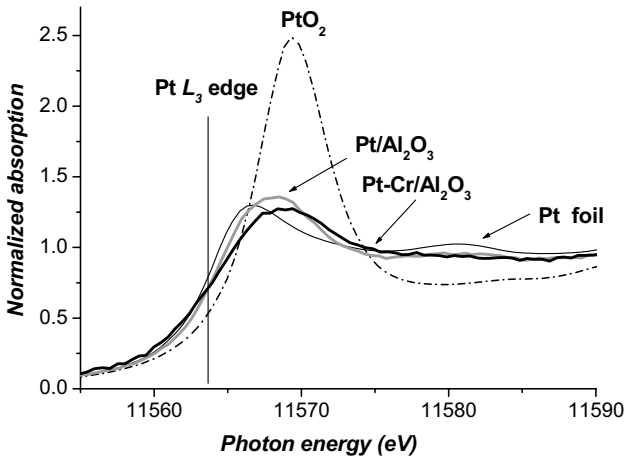

Fig. 1 Pt L_3 XANES spectra of Pt/Al_2O_3, Pt–Cr/Al_2O_3 and reference compounds

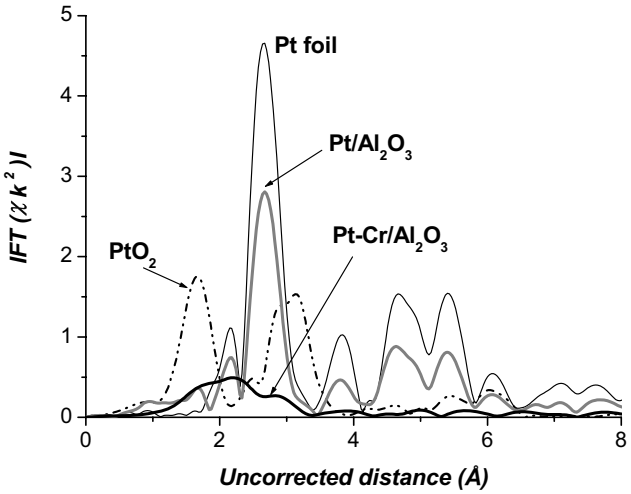

Fig. 2 Pt L_3 EXAFS spectra of Pt/Al_2O_3, $Pt–Cr/Al_2O_3$ and reference compounds

the first peak corresponds to a Pt–O atomic pair, whereas the second peak—to a Pt–Pt atomic pair.

For fitting the EXAFS Pt L_3 edge spectrum of the monometallic Pt sample, crystallographic data of Pt-metal were used. Fitting was done for one shell (double shell) that contains 12 Pt atoms at the 2.807 Å real distance.

The Pt L_3 EXAFS spectrum of the Pt–Cr bimetallic sample was fitted with a two-shell model: Pt–O and Pt–Pt. Crystallographic data of PtO_2 and Pt-metal were used.

The results presented in Table 2 for the Pt/Al_2O_3 and $Pt–Cr/Al_2O_3$ catalysts show the average coordination numbers (CN) and the real distance (r) in atomic pairs. The estimation of the average particle size based on the average coordination number depends on the particle morphology. It should be borne in mind that the estimate of the average size is very approximate.

Using these parameters and with the assumption of a spherical shape, the formal average size (diameter) of Pt particle for Pt/Al_2O_3 catalyst 10–19 Å was obtained. It should be noted that the presence of the long-distance peaks (> 3.5 Å uncorrected distance) (Fig. 2) in the EXAFS spectrum of this sample indicates that the sample contains large particles as well.

Table 2 Best fit of Pt L_3 EXAFS spectra for Pt/Al_2O_3 and $Pt–Cr/Al_2O_3$

Catalysts	Atomic pair	r (Å)	CN	D_{Pt} (Å)
Pt/Al_2O_3	Pt–Pt	2.767 ± 0.005	8.6 ± 0.8	14.5 ± 4.5
$Pt–Cr/Al_2O_3$	Pt–O	2.089 ± 0.003	0.6 ± 0.1	
	Pt–Pt	2.702 ± 0.010	4.6 ± 0.6	6.2 ± 0.6

Fitting the spectrum of the bimetallic sample shows that the local structure of the central absorbing atom consists of 0.6 ± 0.1 O atoms at the 2.089 ± 0.003 Å real distance and 4.6 ± 0.6 Pt atoms at the 2.702 ± 0.010 Å real distance. Using parameters for the Pt–Pt shell, the formal average size (diameter) of Pt particles in the range of 6.2 ± 0.6 Å was obtained.

In addition, the difference in the energy position of the white lines in the Pt L_3 XANES spectra of the foil and two catalysts (Fig. 1) confirms that the real size of the metallic particles follows the order: Pt-foil > Pt/Al_2O_3 > $Pt–Cr/Al_2O_3$.

It should also be noted that the appearance in the nearest environment of the central Pt atom of oxygen as the nearest neighbor nevertheless does not indicate the oxidation of platinum. The Pt L_3 EXAFS spectrum for the sample dehydrated in-situ in a He flow at 120 °C demonstrates the presence of 4–5 oxygen atoms at a distance of 2.043–2.059 Å in the nearest environment of oxidized platinum. At the same time, the distance in the Pt–O atomic pair in the $Pt–Cr/Al_2O_3$ spectrum of the catalyst reduced in an H_2 flow at 350 °C (Table 2) is 2.086–2.092 Å with CN = 0.5–0.7. We suppose that it is caused by the presence of O atoms that are connected with Cr^{3+} cations.

Cr K X-ray absorption near-edge spectra (Fig. 3) of the $Pt–Cr/Al_2O_3$ catalyst demonstrate that the XANES spectrum of the dehydrated sample differs from both Cr foil and Cr_2O_3 and is similar to the spectrum of CrO_3. This finding confirms the existence of Cr^{6+} in a tetrahedral lattice. Reduction of the sample at 350 °C leads to the Cr^{6+} transformation into Cr^{3+} with the following change of the coordination to octahedral.

Fourier transformation of the oscillating part of the spectrum (Fig. 4) that belongs to a dehydrated sample differs from that of both Cr_2O_3 and Cr foil. The EXAFS spectrum of the reduced sample differs from the spectra of all reference compounds and dehydrated sample.

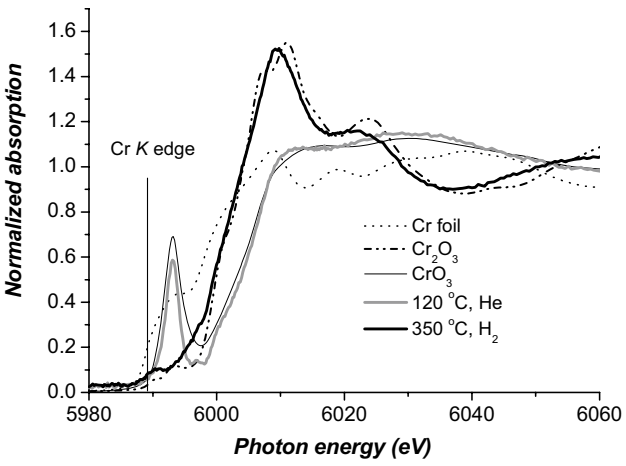

Fig. 3 Cr K XANES spectra of $Pt–Cr/Al_2O_3$ and reference compounds

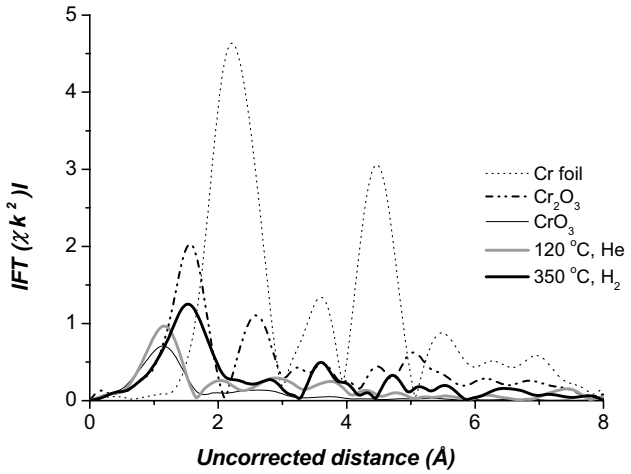

Fig. 4 Cr *K* EXAFS spectra of Pt–Cr/Al_2O_3 and reference compounds

Table 3 Best fit of Cr *K* EXAFS spectra for Pt–Cr/Al_2O_3

Treatments	Atomic pair	*r* (Å)	CN
120 °C, He	Cr–O	1.606 ± 0.008	1.3 ± 0.1
350 °C, H_2	Cr–O	1.977 ± 0.012	3.6 ± 0.3
	Cr–Cr	3.080 ± 0.001	0.4 ± 0.2

The results presented in Table 3 for the Pt–Cr/Al_2O_3 catalyst present the average coordination numbers (CN) and the real distance (r) in the first and second coordination spheres obtained by EXAFS spectra fitting using the scattering amplitude and phase of Cr_2O_3 and CrO_3. Best-fit results for the dehydrated catalyst are comparable with the characteristics of CrO_3. The crystallographic data of CrO_3 consists of 1-st shell (Cr–O atomic para with CN = 1 at 1.575 Å), 2-nd shell (Cr–O with CN = 1 at 1.579 Å), 3-d shell (Cr–O with CN = 2 at 1.748 Å). For fitting we used 1-st shell only.

On the contrary, the coordination number obtained for the reduced sample is lower and the real distance is larger compared with the characteristics of Cr_2O_3. This fact argues the existence of isolated Cr^{3+} ions, i.e. a Cr_2O_3 phase does not form during the reduction. As to the distribution of Cr relative to Pt, we suppose that the presence of Cr results in Pt dilution. At this stage of research, we do not have any evidence of the Pt–Cr interaction that is required for the alloy formation. Thus, chromium ions introduced in the Pt/Al_2O_3 catalyst provide conditions for stabilization of smaller Pt nanoparticles that are more active in the dehydrogenation of perhydro-*N*-ethylcarbazole.

4 Conclusions

It has been found that a decrease of the Pt^0 particle size in the Pt–Cr/Al_2O_3 catalyst compared with Pt/Al_2O_3 promotes an increase of the catalytic activity in the perhydro-*N*-ethylcarbazole dehydrogenation reaction. Thus, the use of bimetallic catalysts in reversible hydrogenation–dehydrogenation of heteroaromatic substrates can boost the performance of hydrogen storage. The further perspectives in designing efficient catalytic systems for the application in hydrogen storage based on reversible hydrogenation–dehydrogenation of aromatic substrates may be related to the use of hybrid nanomaterials, including core–shell nanoparticles supported onto mesoporous supports [11, 12].

Acknowledgements The work was carried out with a financial support from the Ministry of Education and Science of the Russian Federation in the framework of Increase Competitiveness Program of NUST «MISiS» (No. K2-2017-011) in the part related to the preparation of catalysts and to Russian Science Foundation (Grant No. 14-50-00126) in the part related to the characterization and catalytic studies.

References

1. Crabtree RH (2008) J Energy Environ Sci 1:134–138
2. Eberle U, Felderhoff M, Schuth F (2009) Angew Chem Int Ed 48:6608–6630
3. Moores A, Poyatos M, Luo Y (2006) New J Chem 30:1675–1678
4. Sotoodeh F, Smith KJ (2010) Ind Eng Chem Res 49:1018–1026
5. Sotoodeh F, Zhao L, Smith KJ (2009) Appl Catal A 362:155–162
6. Sotoodeh F, Smith KJ (2011) J Catal 279:36–47
7. Klementiev KV VIPER for Windows (Visual Processing in EXAFS Researches), freeware, http://www.cells.es/Beamlines/CLAESS/software/viper.html
8. Ankudinov AL, Ravel B, Rehr JJ, Conradson SD (1998) Phys Rev B 58:7565–7576
9. Borowski M (1997) J Phys IV 7:C2259–C2260
10. Stakheev AYu, Tkachenko OP, Kapustin GI, Telegina NS, Baeva GN, Brueva TR, Klementiev KV, Gruenert W, Kustov LM (2004) Russ Chem Bull 3:502–511
11. Ananikov VP, Gordeev EG, Egorov MP, Sakharov AM, Zlotin SG, Redina EA, Isaeva VI, Kustov LM, Gening ML, Nifantiev NE (2016) Mendeleev Commun 26:365–374
12. Ananikov VP, Eremin DB, Yakukhnov SA, Dilman AD, Levin VV, Egorov MP, Karlov SS, Kustov LM, Tarasov AL, Greish AA, Shesterkina AA, Sakharov AM, Nysenko ZN, Sheremetev AB, Stakheev AYu, Mashkovsky IS, Sukhorukov AYu, Ioffe SL, Terent'ev AO, Vil' VA, Tomilov YuV, Novikov RA, Zlotin SG, Kucherenko AS, Ustyuzhanina NE, Krylov VB, Tsvetkov YuI, Gening ML Nifantiev NE (2017) Mendeleev Commun 27:425–438